RSC Advances

ROYAL SOCIETY OF CHEMISTRY

www.rsc.org/advances

Structural and Electronic Properties of the $PbCrO_4$ Chrome Yellow Pigment and of Its Light Sensitive Sulfate-Substituted Compounds

Anna Amat,[a,b] Costanza Miliani,[b] Simona Fantacci [a,b,*]

[a] Computational Laboratory for Hybrid/Organic Photovoltaics (CLHYO), CNR-ISTM, via Elce di Sotto 8, 06123 Perugia, Italy.

[b] CNR-ISTM, via Elce di Sotto 8, 06123 Perugia, Italy.

ABSTRACT: Chrome Yellows (CY) are a family of synthetic pigments of formula PbCr(1-x)SxO4, used by van Gogh and other nineteenth-century masters, whose photo-degradation threatens the conservation of invaluable works of art. Experimental studies have demonstrated that the darkening of the pigment is provoked by the formation of superficial layers of Cr(III) oxides and sulfates due to the reduction of the native Cr(VI) to the Cr(III) oxidation state. A strong correlation between CY degradation and its chemical composition (sulfate richness) and structure (orthorhombic vs. monoclinic) was also experimentally put forward. Here we investigate a possible sulfate pathway to CY degradation, and investigate PbCr(1-x)SxO4 (x=0, 0.25, 0.5, 0.75, 1) compounds in both orthorhombic and monoclinic phases by first principles DFT calculations. Our results show that the mixed PbCr(1-x)SxO4 and the native PbCrO4 share a similar electronic structure , though an energy up-shift of the conduction band is computed by both increasing the amount of sulfate and passing from the monoclinic to the orthorhombic phase. Our calculations suggests that, under a purely electronic picture, the Cr(VI) photo-reduction is more difficult for compounds with high sulfur concentration and an orthorhombic phase. Therefore, we conclude that degradation should be ascribed to other factors, such as different solubility and morphology.

1. Introduction

Chrome Yellows (CY) are a family of synthetic yellow pigments of $PbCr_{(1-x)}S_xO_4$ formula, which have been introduced in 1809 by Vaquelin and made commercially available since around 1815.[1, 2] CY suddenly entered in the palette of nineteenth-century masters, including J. Constable,[3] J. M.W Turner,[4] V. van Gogh,[5, 6] G. Seraut,[7] C. Pissarro,[8] P. Cezanne,[9] J. Ensor,[10] which highly appreciated its bright and opaque colour ranging from deep yellow to lemon yellow. Pure $PbCrO_4$ is the reference compound, CrO_4^{2-} being responsible for the characteristic deep yellow colour of the pigment; it shows a monoclinic crystal structure (Scheme 1, left). Upon substitution of chromate anions with sulphates, the colour of $PbCr_{(1-x)}S_xO_4$, solid solutions gradually shifts towards lemon yellow while the structure changes from the monoclinic to the orthorhombic phase typical of $PbSO_4$. Sulphate-poor CY pigments, with $x < 0.4$, maintain a prevalence of monoclinic phase while the orthorhombic phase prevails by further increasing the sulphate amount, since the pure $PbSO_4$ only exists in the orthorhombic anglesite-type crystal structure (see Scheme 1, right).

A number of paintings where CY were employed, comprising some iconic works by Van Gogh, have shown with time a perceptible darkening of colour which raises serious concerns for their conservation. The penchant for degradation of chromate-based pigments has been extensively investigated in the last few years by employing synchrotron radiation (SR)-based X-ray microprobe techniques as well as electronic and vibrational spectroscopies on both original paint micro-samples and artificially aged paint models.[11-21] It has been found that the pigment darkening is likely due to the formation of a superficial micrometric layer made of amorphous Cr(III) oxides (Cr_2O_3) along with Cr(III) sulphates and/or organometallic Cr(III) compounds; the alteration process has been accordingly ascribed to reduction of the native Cr(VI) to the Cr(III) oxidation state.

Both environmental (light, temperature, humidity) and intrinsic (composition of the CY solid solution, paint additives, organic binding media) aspects have been evaluated as potential triggering factors of the formation of superficial Cr(III)-compounds.[11,14,15,16,19,21] It has been proved that the reduction process is mainly photo-activated (by both UV and visible light), although a role can be played also by Cr(V) intermediate compounds thermally formed by interaction of CY with the binding medium (typically a drying oil). [19, 21] Behind these environmental factors it has emerged, however, that the primary role is ascribable to the chemical composition and structure of $PbCr_{(1-x)}S_xO_4$ solid solutions. As a matter of fact, orthorhombic sulphate-rich CY are much more prone to photochemical reduction than the sulphate-poor analogues having a monoclinic crystal phase.[14,19]

To shed some light on the nature of the material structure/properties relationship and to analyze how the electronic structure of CY is affected by compositional and structural changes, here we investigate the CY pigment and its sulphate-substitution products by first principles electronic structure computational analyses. Theoretical

modeling can provide accurate information at the microscopic level of colouring materials used in paintings[22-30] and in different applications.[31-38] In this study, we have taken into account well defined models and have investigated the interplay between structural and electronic properties as a function of the composition and the crystalline phase. The pure $PbCrO_4$ and $PbSO_4$ reference structures have been investigated by employing Density Functional Theory (DFT) calculations, including both scalar relativistic (SR) and spin-orbit coupling (SOC) effects. After having tested different levels of theory on the reference lead chromate and sulphate compounds, we have focused on the intermediate binary structures $PbCr_{(1-x)}S_xO_4$ with x=0.25, 0.50 and 0.75, in both monoclinic (m-$PbCr_{(1-x)}S_xO_4$) and orthorhombic (o-$PbCr_{(1-x)}S_xO_4$) phases. These theoretical models can be related to the CY laboratory synthesized samples, with increasing amount of sulphate and proved to have different grades of light fastness.[31-38] Our study shows that due to the peculiar electronic structure of $PbCrO_4$ and of the related $PbCr_{(1-x)}S_xO_4$, the Cr(IV) to Cr(III) reduction process becomes less energetically favored for sulphate-rich species or within the orthorhombic phase, thus suggesting that the role of sulphate in the degradation is possibly limited to factors different from pure electronic ones, such as its different solubility and morphology (i.e. smaller particle size).

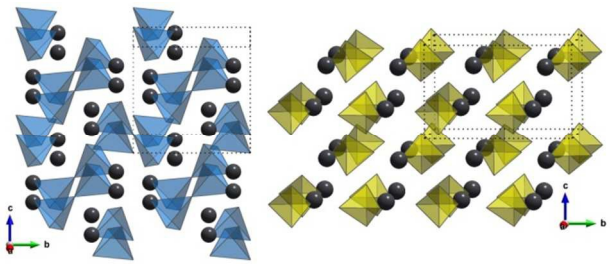

Scheme 1. Left: $PbCrO_4$ in monoclinic (P121n1) phase. Right: $PbSO_4$ in orthorhombic (Pbnm) phase.

2. Models and Computational Details

All the calculations have been carried out using the PWSCF code as implemented in the Quantum-Espresso program package, without any symmetry constraint.[39] The PBE exchange-correlation functional was used and the electron-ion interactions were described by ultrasoft pseudopotentials (USPP) from the Pslibrary.[40] Pb 5d, 6s and 6p electrons; Cr 3s, 4s, 3p and 3d; S 3s and 3p; O 2s and 2p shells were explicitly included in the calculations. Plane-wave basis set cutoffs of 50 Ry and 400 Ry were used for the smooth part of the wavefunctions and the augmented density, respectively. Both scalar relativistic (SR) and full relativistic calculations including spin-orbit coupling (SOC) have been performed. A 4x4x4 Monkhorst Pack grid[41] was used to sample the Brillouin zone of the tetragonal systems.

We optimized the structure of $PbCrO_4$ using as reference the available experimental data. At room temperature $PbCrO_4$ assumes a P121n1 monoclinic phase (m-$PbCrO_4$)[42] while at high temperatures an orthorhombic (Pnma) structure (o-$PbCrO_4$) has been reported[43] very similar to that of $PbSO_4$ (o-$PbSO_4$), which is found in an anglesite structure with an orthorhombic conformation (Pbnm), see Scheme 1.[44] Since a similar change of phase, from the monoclinic to the orthorhombic, has been observed for the mixed systems upon increase the sulfur concentration, the electronic properties of the o-$PbCrO_4$ and o-$PbSO_4$ have also been investigated and compared to that of m-$PbCrO_4$.

The investigated cells of $PbCrO_4$ and $PbSO_4$ contain a total of 24 atoms: 4 Pb, 4 Cr/S and 16 O. The cell of m-$PbCrO_4$ has an angle β of 102.42° while the α and γ angles are equal to 90°. The a and b cell parameters are measured 7.12 and 7.34 Å, respectively, while c is 6.79 Å, being the total volume of the cell 350.80 Å^3. The orthorhombic phase of this species, o-$PbCrO_4$, is slightly larger, 367.00 Å^3 is the cell volume and a, b and parameters measure 8.80, 5.73 and 7.27 Å, respectively. o-$PbSO_4$ is very similar to the analogous chromate, showing smaller a, b and c parameters 6.96, 8.48 and 5.40 Å, respectively, accounting for a total volume of 318.49 Å^3.

Geometry optimization of these structures has been performed both by leaving the cell parameters fixed at the experimental values and optimizing the ions (experimental cell), and by allowing both the cell and the ions to relax (optimized cell). Calculations have been performed using a SR-DFT approach and a full relativistic one, including SOC effects. To investigate how the changes in the chemical composition and crystalline phase are reflected on the electronic structure of CY, we have taken into consideration mixed Cr and S materials (i.e. $PbCr_{(1-x)}S_xO_4$) which have also experimentally studied.[14, 18, 19,21, 45, 46] We investigated mixed structures with composition range x=0, 0.25, 0.5, 0.75, 1; for the x=0.5 substitutions we have taken into account the three possible distributions of the CrO_4^{2-} and SO_4^{2-} octahedra in the crystal, see discussion below. The compounds have been modeled by subsequently replacing the chrome by sulfur atoms in the m-$PbCrO_4$ structure and re-optimizing both cell and ions for the monoclinic phase, and making the reverse process (substitution of sulphate by chromate) starting from o-$PbSO_4$ for the orthorhombic phase.

3. Results and Discussion

3.1 $PbCrO_4$ and $PbSO_4$ reference structures

In Figure 1 the SOC-optimized structures of m-$PbCrO_4$, o-$PbCrO_4$ and o-$PbSO_4$ are reported. Negligible differences have been computed in the optimized geometrical parameters obtained using the experimental and optimized cell parameters, with the exception of o-$PbCrO_4$ that is not stable at room temperature [47, 48] and indeed undergoes a strong reorganization upon cell relaxation (see Supporting Information). The inclusion of SOC only slightly affects the optimized structures suggesting that SOC has a minor impact on the geometry of the investigated systems (see Supporting Information).

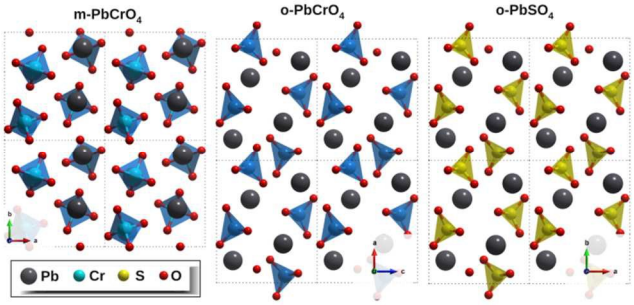

Figure 1. Optimized structures of m-$PbCrO_4$ (P121n1), o-$PbCrO_4$ (Pnma) and o-$PbSO_4$ (Pbnm).

The SOC-DFT band structures calculated on the optimized geometries employing experimental cell parameters are reported in Figure 2, see Supporting Information for the corresponding SR-DFT data. A summary of indirect and lowest direct band gaps are reported in Table 1.

Table 1. Direct and indirect band gaps (eV) computed for m-$PbCrO_4$, o-$PbCrO_4$ and o-$PbSO_4$ using SR- and SOC-DFT. Band gaps have been computed employing the experimental cell parameters and upon atomic+cell parameters optimization.

		m-PbCrO4		o-PbCrO4		o-PbSO4	
		Exp. Cell.	Opt. Cell.	Exp. Cell.	Opt. Cell.	Exp. Cell.	Opt. Cell.
SR	Dir.	1.81 (A-B) 1.82 (A)	1.79 (A-B) 1.81 (A)	1.96 (Γ)	1.53 (Γ)	4.29 (U) 4.55 (Γ-Z)	4.29 (Γ-Z) 4.56 (U)
	Ind.	1.73	1.71	1.96		1.52	
SOC	Dir.	1.74 (A-B) 1.75 (A)	1.71 (A-B) 1.72 (A)	1.86 (Γ)	1.45 (Γ)	3.81 (U) 3.82 (Γ-Z)	3.81 (Γ-Z) 3.82 (U)
	Ind.	1.65	1.63	1.85	1.44	3.59	3.59

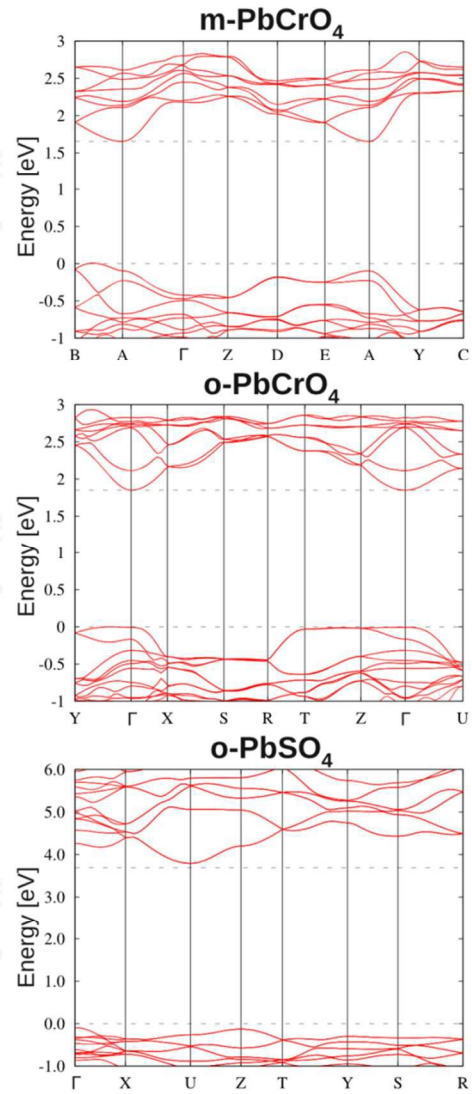

Figure 2. SOC-DFT band structures of m-$PbCrO_4$, o-$PbCrO_4$ and o-$PbSO_4$ employing the experimental cell parameters. The zero has been set in both cases at the top of the valence band.

An indirect band gap of 1.73 and 1.65 eV is computed for m-$PbCrO_4$ using SR- and SOC-DFT, respectively. SOC thus induces a small (0.08 eV) decrease in the computed band gap suggesting a moderate involvement of the lead atoms in the band edges. On overall, the results are quite underestimated with respect to the experimental ones reported at ca. 2.3 eV[49] as expected for standard GGA-DFT calculations.[50-52] The top of the valence band is computed between A and B while the bottom of the conduction band is computed at A, the direct band gap in A lays ca. 0.10 eV above the indirect one. The presence of a direct band gap close to the indirect band gap is in line with the previous computational analyses by Errandonea et al.[49, 53] who found m-$PbCrO_4$ to be an indirect band gap semiconductor, with the direct band gap easily accessible. As it can be noticed from Table 1, the differences between the band gaps computed using the experimental cells or the optimized ones are negligible.

The band gap of o-$PbCrO_4$ is computed to be 1.96 and 1.86 eV by SR- and SOC-DFT, respectively. Here the band gap can be considered as being direct at the Γ point of the Brilluoin zone, almost degenerate with the computed indirect ones. Upon cell relaxation, the orthorhombic phase slightly deviates from orthogonality and while the b axis remains unchanged, the a and c axis are reduced and increased by 8% and 6%, respectively, resulting in a total reduction of the volume of ca. 4%. Structural changes lead to a dramatic drop of the band gap by as much as 0.4 eV, bringing it below that of the monoclinic phase. These variations are not surprising when considering that o-$PbCrO_4$ has been only reported at high temperatures and is not stable at standard conditions. The band gap of the relaxed cell structure is still computed at Γ and the structure of the band is very similar to that computed for the experimental cell, with a very flat region of the valence band and a clear minimum of the conduction band at Γ.

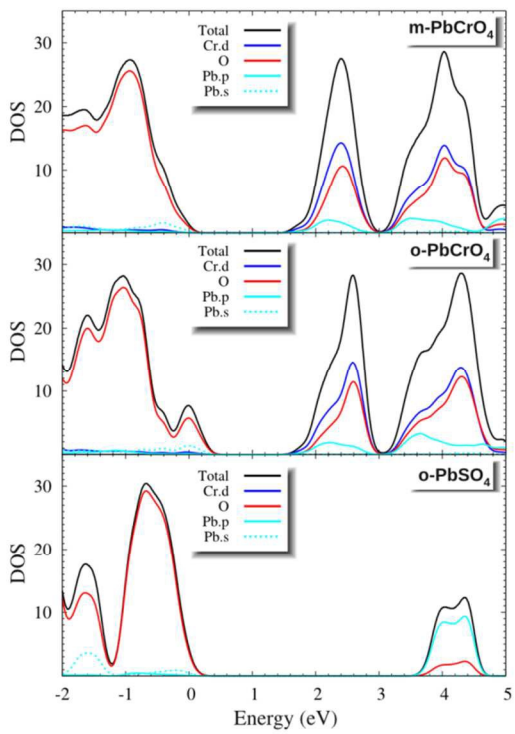

Figure 3. Total density of states for m-$PbCrO_4$ (top), o-$PbCrO_4$ (middle) and the o-$PbSO_4$ (bottom) structures. Contribution of the main orbitals to the valence and conduction bands. The DOS have been aligned using the Pb d peaks (spin down) and the zero has been set to the top of the m-$PbCrO_4$ valence band.

The indirect band gap of o-$PbSO_4$ is 4.05 and 3.59 eV by SR- and SOC-DFT, respectively, and lays ca. 0.2 eV below the lowest direct band gap computed at U. The bottom of the conduction band is computed at U while the top of the valence band is computed between Γ and Z. In o-$PbSO_4$ SOC lowers the band gap by ca. 0.5 eV, a stronger effect than what found for $PbCrO_4$ due to the larger Pb character of the conduction band with respect to the lead chromates, as discussed below. The SOC-DFT band gap is overestimated by ca. 0.4 eV with respect to the experimental one, reported at ca. 3.2 eV.[54] While the origin of such overestimate is presently not clear, we notice that a similar discrepancy was found for similar oxides.[49, 53]

The density of states (DOS) of the investigated pure phases is reported in Figure 3. The valence band has a similar composition for the three compounds and is mainly due to the oxygen orbitals, with a minor involvement of the Pb s orbitals, a contribution which decreases passing from m-$PbCrO_4$ to o-$PbCrO_4$ and o-$PbSO_4$. The valence band of o-$PbCrO_4$ phase is up-shifted by ca. 0.25 eV with respect to the monoclinic phase (alignment done considering the Pb 5d states), it is shown as a more structured band with a higher energy low intensity peak. This up-shift in the o-$PbCrO_4$ valence band is responsible for the decrease of the band gap discussed previously and it is due to the structural reorganization and the decrease of the cell volume. This is confirmed by looking at the valence band structure of o-$PbCrO_4$ using the experimental cell parameters, which does not show a band gap lowering, see Supporting Information.

The conduction band of $PbCrO_4$, in both crystalline phases shows mainly contributions from Cr d orbitals and O p orbitals and a low but meaningful amount of Pb p states. In o-$PbSO_4$, the conduction band is essentially delocalized on the Pb and O centers and is up-shifted by ca. 2 eV with respect to $PbCrO_4$. This change reflects in an opening of the band gap as experimentally found to go from 2.3 eV for m-$PbCrO_4$ to 3.2 eV for o-$PbSO_4$. The larger involvement of lead atoms in the conduction band of $PbCrO_4$ than in o-$PbSO_4$ accounts for the larger SOC effects computed for the sulphate with respect to the chromate analogue, as discussed above. A conduction band character similar to that of o-$PbSO_4$ has been also observed for $PbMoO_4$ and $PbWO_4$, both in the related tetragonal crystal structure, both showing a larger experimental band gap than $PbCrO_4$, 3.3 and 3.9 eV, respectively.[53]

The electronic structure of $PbCrO_4$ presents a few peculiarities with respect to the previous cited metal oxides. The CrO_4^{2-} ion shows a weaker crystal field splitting compared to the MoO_4^{2-} and WO_4^{2-} tetrahedral anions. The antibonding combination of the Cr d orbitals and oxygen lone-pairs lies at lower energies with respect to the unoccupied localized Pb states, thus becoming the final states of charge transfer excitations. In addition, the Pb contribution to the conduction band of $PbCrO_4$ seems to have implications on the CY pigment colour. This contribution is obviously absent in $SrCrO_4$, an oxide in the monazite crystal structure, which, even presenting similar contributions of Cr and O in the valence and conduction bands, has a larger band gap with respect to the analogue Pb ternary oxide.[53] The Pb presence in the conduction band is due to hybridization of deep occupied Pb and O states; and the antibonding Pb-O component shifts to lower energies the conduction band, mainly of Cr-O character, making it more accessible and easier to be (photo) reduced. In the case of sulphate the Pb character of the conduction band changes completely the nature of

charge-transfer transitions and the chemical-physical properties of this compound.

3.2 Mixed PbCr(1-x)SxO4 structures

The pathway to gradually replace chromate with sulfate anions in monoclinic $PbCrO_4$ has been simulated to elucidate how the introduction of an increasing amount of sulfate may influence the structural and electronic proprieties of CY.[14, 18, 19] Mixed Cr/S structures of formula m-$PbCr_{(1-x)}S_xO_4$ (with x = 0.25, 0.5, 0.75) have been analyzed. Since experimentally a change of phase from monoclinic to orthorhombic is observed when synthesizing lead chromate in the presence of more than 50% of sulfur, we optimized the mixed o-$PbCr_{(1-x)}S_xO_4$ materials and the analogous monoclinic phase. The monoclinic and orthorhombic optimized structures are reported in Figure 4. The mixed structures are formed by CrO_4^{2-} and SO_4^{2-} tetrahedra with a nine-fold coordination of the Pb in distorted polyhedra. We compute very similar stabilities and electronic parameters for the three considered x=0.5 structures, see Supporting Information. Therefore hereafter only the most stable conformation of both phases (c) will be reported. In Table 2 the optimized main cell parameters and the valence and conduction band edges relative to those of m-$PbCrO_4$ are reported.

Upon increasing the amount of sulfur a reduction of the cell volume is predicted, nicely matching the experimental observations; [55, 56] the volume contraction is 5% for the monoclinic phase, while for the orthorhombic phase the volume contracts by 9%. To get insight into the possible changes of the structural parameters which accompany the substitution of chromate with sulfate, the PbO, CrO and SO distances of the polyhedrons have been analyzed but no relevant effects have been noticed, Supporting Information.

The band gap is strongly influenced by the presence of sulfur. For the monoclinic phase the band gap increases by 0.21 eV (x=0.25), 0.35 eV (x=0.50) and 0.46 eV (x= 0.75) with respect to $PbCrO_4$, while the band gap of the orthorhombic phase markedly increases by 0.30, 0.64 and 0.71 eV for x=0.25, 0.50 and 0.75, respectively, see Table 2. Despite the known flaws of PBE in computing absolute band gap energies, we are confident that the methodology is accurate enough to qualitatively, at most, reproduce the band gap evolution as a function of sulphate richness. For pure m-$PbSO_4$ (o- PbSO4) the band gap is computed to be 2.22 eV (2.09 eV) larger than that of m-$PbCrO_4$ (o-PbCrO4) due to a completely different conduction band composition, in line with that discussed above for the pure phases. For the mixed monoclinic structures, the valence band is stabilized by 0.10 eV with respect to the pure m-$PbCrO_4$, while the conduction band is progressively up-shifted by increasing the sulfur amount, see Table 2, being both shifts responsible of the band gap opening. The same trend is found for the orthorhombic species.

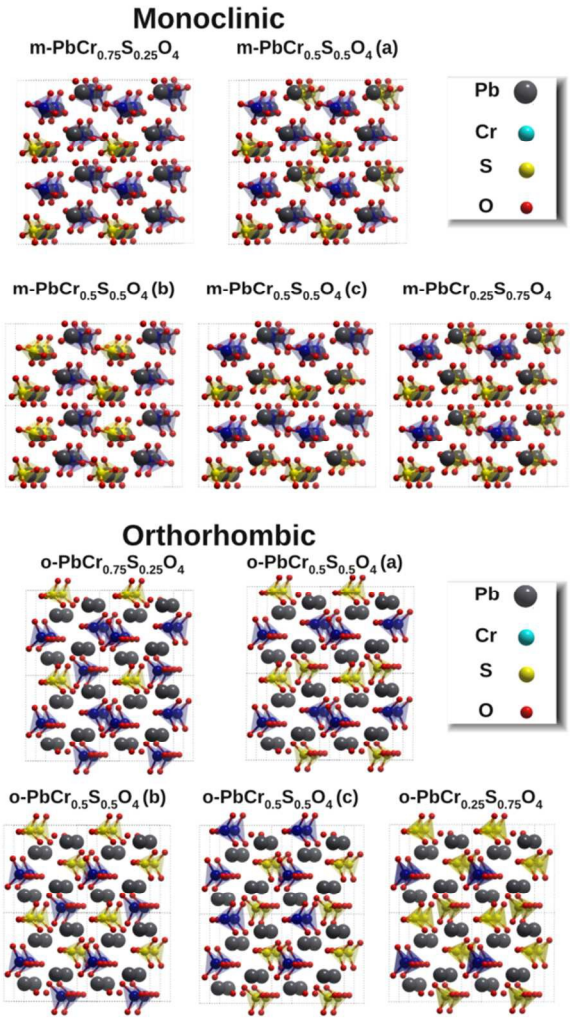

Figure 4. Optimized structures of the investigated mixed m-$PbCr_{(1-x)}S_xO_4$ and o-$PbCr_{(1-x)}S_xO_4$

Except for the conduction band of $PbSO_4$, the valence and conduction bands of the orthorhombic structures are up-shifted with respect to their monoclinic counterparts. For the valence band we computed shifts in between 0.2-0.3 eV, while the variations of the conduction band is far more pronounced, see Table 2. It can be noticed that the conduction band of the reference pure species are very similar in both crystalline phases, with computed differences below 0.1 eV, while for x=0.25, 0.50 and 0.75 we compute an up-shift of 0.25, 0.38 and 0.37 eV, respectively, of the conduction band going from monoclinic to orthorhombic phase, see Table 2. These changes deliver band gaps in the orthorhombic phase that are lower for x=0 (-0.13 eV) and x =1 (-0.26 eV) compared to their monoclinic counterparts, while they are almost unchanged for x=0.25 and larger for x=0.5 and x=0.75, in line with the experimental findings,[19] see Supporting Information.

Table 2. Computed cell parameters, band gap (SR and SOC) and position of the top and bottom of the valence and conduction bands, respectively, for the m-$PbCr_{(1-x)}S_xO_4$ and o-$PbCr_{(1-x)}S_xO_4$ structures. The electronic structures have been aligned using the Pb d (spin down) peak taking as reference that of the m-$PbCrO_4$ and zero has been set to the top of the valence band of m-$PbCrO_4$.

	m-$PbCr_{(1-x)}S_xO_4$					o-$PbCr_{(1-x)}S_xO_4$				
	x=0	x=0.25	x=0.5	x=0.75	x=1	x=0	x=0.25	x=0.5	x=0.75	x=1
Volume (Å^3)	2351	2319	2293	2261	2232	2354	2280	2221	2181	2141
A (Å)	7.107	7.097	7.066	7.034	7.000	7.633	7.414	7.178	7.188	7.124
B (Å)	7.427	7.376	7.344	7.297	7.259	8.391	8.503	8.691	8.622	8.632
C (Å)	6.762	6.726	6.715	6.692	6.669	5.835	5.741	5.653	5.587	5.530
A (°)	89.9	89.8	90.0	90.0	90.0	90.0	90.0	90.0	89.7	90.0
B (°)	102.5	102.6	102.8	102.7	102.6	90.0	90.0	90.0	90.0	90.0
Γ (°)	90.1	90.4	90.0	89.9	90.1	90.0	90.0	90.0	90.0	90.0
VB (eV)	0.00	-0.10	-0.11	-0.12	-0.10	0.21	0.19	0.08	0.13	0.10
CB (eV)	1.63	1.74	1.84	1.97	3.75	1.71	1.99	2.22	2.34	3.69
Egap (eV)	1.63	1.84	1.95	2.09	3.85	1.50	1.80	2.14	2.21	3.59

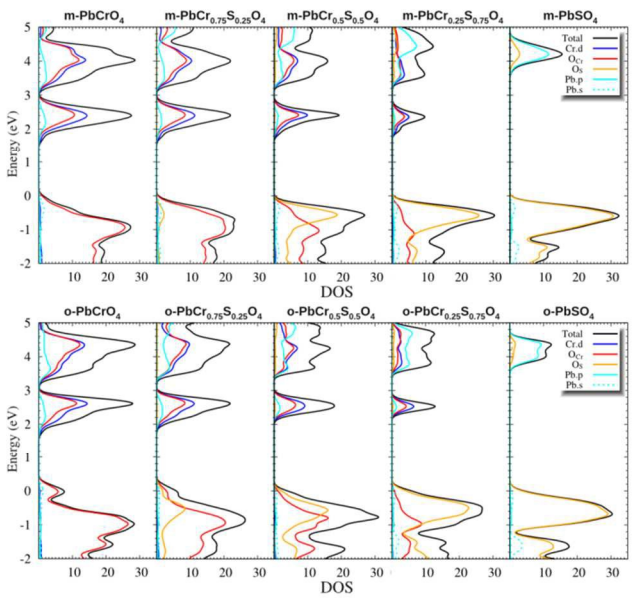

Figure 5. Total and projected density of states for the m-$PbCr_{(1-x)}S_xO_4$ and o-$PbCr_{(1-x)}S_xO_4$ structures. Contribution of the main orbitals to the valence and conduction bands. PDOS have been aligned using the Pb.d (spin down) peak taking as reference that of m-$PbCrO_4$. The zero has been set to the top of the valence band of m-$PbCrO_4$. O_{Cr} and O_s are referred to the oxygen bonded to Cr and S, respectively.

The total and projected DOS of the investigated oxides are reported in Figure 5. Since the oxygen atoms of chromate and sulfate are not electronically equivalent, we have analyzed separately those belonging to the CrO_4^{2-} tetrahedra, hereafter O_{Cr}, from those coming from SO_4^{2-}, hereafter O_S. On overall, for the mixed m-$PbCr_{(1-x)}S_xO_4$ species the valence band is mainly composed of p orbitals of both O_{Cr} and O_S in different ratios depending on the composition, with a small contribution from Pb s orbitals.

The composition of the conduction band of the mixed species is quite stable with the progressive substitution of chromium by sulfur and show almost exclusively contributions from the O_{Cr} p and the Cr d states with a minor participation of the Pb p orbitals, analogously to that found for the reference m-$PbCrO_4$. For the m-$PbCr_{(1-x)}S_xO_4$ species, we therefore find, up to a minimal Cr concentration (0.25), a conduction band up-shifted with respect to pure m-$PbCrO_4$ due to the reduced density of the contributing Cr states. In m-$PbSO_4$ the composition of the conduction band completely differs from that containing chromium being mainly due to the Pb p orbitals, as discussed above for the orthorhombic phase, o-$PbSO_4$.

To analyze in details the partial DOS (PDOS) of the mixed species, the areas of the PDOS with respect to the total DOS in defined regions of energy have been integrated (see the integration limits in Supporting Information) and expressed in percentages with reference to the total areas of the accounted band. For the monoclinic phase, in the region of the valence band in between ca. -1.2 and 0.4 eV PDOS of O_S contribute for 0%, 6%, 49 %, 72% and 93% to the total DOS going from x=0 to x=1 while the PDOS of O_{Cr} contribute for 89%, 84%, 42%, 19% and 0, showing a good correlation with the CrO_4^{2-} amount in the crystalline cell. The contribution of Pb 6s orbitals in this energy region is constant at ~5%. In the conduction band region between ca. 1.5 and 3 eV, for all the species containing CrO_4^{2-}, the PDOS of Cr is constant contributing 51-52%, independently from the amount of CrO_4^{2-}, also the PDOS of O_{Cr} consistently contribute to the conduction band (36-31%) while the Pb d orbitals contribute for 8%. This Pb contribution is originated from the antibonding counterpart of the Pb - O_{Cr} mixing induced by Cr, as discussed for m- $PbCrO_4$, and is therefore not present for $PbSO_4$. Indeed, for the PDOS of m-$PbSO_4$ only a single band at ca. 10.2 eV is observed, 93% O_S p and

7% Pb, whose character is similar to that of the orthorhombic phase.

For the o-$PbCr_{(1-x)}S_xO_4$ systems, the highest-energy peak in the valence band, characteristic of the total DOS o-$PbCrO_4$ structure is maintained, even though smoothed, only for the species with x=0.25. The valence band character is essentially oxygen and in the intermediate mixed species the composition in terms of O_{Cr}/O_S reflects the ratio of chromate/sulfate of the considered system. For the o-$PbCr_{(1-x)}S_xO_4$ species (x=0.00-0.75), we evaluated the contribution of the Cr, O and Pb by integrating the conduction band areas of the PDOS, with integration limits 1.5-3.0 eV. The Cr states constantly contribute for ~51% to the conduction band of all the oxides, 37-35% is the contribution of O_{Cr}, and 9-10% is that of Pb. It is interesting to notice that independently to the presence of S or Cr, the character of the conduction band of the mixed o-$PbCr_{(1-x)}S_xO_4$ species (x=0.0-0.75) is the same, analogously to that observed for the monoclinic phase; we observe only a decrease in the density of the Cr and O_{Cr} states.

The composition of the orthorhombic valence and conduction bands is very similar to that retrieved for the monoclinic structure, the up-shift of the conduction band is essentially related to the lower number of Cr and O_{Cr} states contributing to the conduction band and this decrease is probably related to the lightening of the CY pigment by increasing the amount of sulfate.[14] Incidentally, SR-DFT calculations provide a qualitatively similar electronic properties as calculated including spin-orbit coupling, see Supporting Information.

On overall, our calculations do not show any peculiar electronic features between monoclinic and orthorhombic series which could explain the different inclination to degradation. We therefore believe that other reasons, probably related to the morphology of the materials, make the orthorhombic phase, with an amount of SO_4^{2-} larger than x=0.4, more prone to photo-induced blackening.

4. Summary and Conclusions

We have investigated the interplay of structural, chemical composition and electronic factors in determining the properties of the Chrome Yellow (CY) pigments. $PbCr_{(1-x)}S_xO_4$ compounds (x=0, 0.25, 0.5, 0.75 and 1) have been taken into account both in a monoclinic and an orthorhombic phase. To shed some light on the reduction of chrome from Cr(VI) to Cr(III) that takes place at high sulfur concentration and that is associated to the pigment darkening we have investigated in depth the changes of the structural and electronic properties of the studied species. The band gap of the lightfast and deep yellow m-$PbCrO_4$ reveals that the valence band is mainly composed by O with minor contributions of the Pb s orbitals, while the conduction band is instead formed by Cr d and O p orbitals with a small contribution from the Pb p orbitals. The introduction of sulfur leads to a slight decrease of the volume cell and a progressive increase of the band gap, which accounts for the shift of color toward lemon yellow. In all the mixed species, the composition of the valence and conduction bands are very similar to that of pure m-$PbCrO_4$. Interestingly, while both the oxygen bounded to sulfur and to chromium participate in the valence band, only those from the CrO_4^{2-} octahedra are involved in the conduction band. The conduction band of $PbSO_4$, stable in the orthorhombic phase, has an obviously different character being mainly contributed by Pb p orbitals. An energy upshift of ca. 2 eV compared to that of m-$PbCrO_4$ is associated to this compositional change. The orthorhombic phase of the mixed species also shows an increase of the band gap upon increasing the amount of sulfur. The band gap of o-$PbCr_{(1-x)}S_xO_4$, is lower, equal and higher than their monoclinic counterparts for x=0, 0.25 and >0.5, respectively. The compositions of the bands are very similar to those of their monoclinic counterparts but the conduction band shows a progressive increase/decrease of the p O_{Cr}/Pb orbitals.

Both the introduction of sulfur and the change of phase induce an up-shift of the conduction band. Taking the top of the conduction band as an estimate of the material reduction potential, our data suggest that (photo) reduction becomes more difficult for the species with high sulfur concentration or with an orthorhombic phase. On overall, we can conclude that in a purely electronic picture, $PbCrO_4$ is more prone to light induced reduction than the sulfate analogues. A possible explanation of the higher light sensitivity of sulfate-rich CYs (x>0.4) pigments may then lay in an higher tendency to release CrO_4^{2-} anions into the paint matrix which could be the actual responsible of the photoredox process experimentally observed. Thus, other properties of the $PbCr_{(1-x)}S_xO_4$ system will be modeled such as the effect of sulfate substitution on both thermodynamic and kinetic solubility of the pigment into the organic binding medium. We hope that our study, providing a quantitative description of the electronic structure of the pigment models, being able to follow how the electronic properties respond to compositional and structural modifications, may complement the analytical and spectroscopic data and provide an alternative perspective in the pigments analysis.

ASSOCIATED CONTENT

Supporting Information. Cell parameters for the experimental and optimized cells. Relative stabilities of the m- o-PbCro.5So.5O4 compounds. Band structure and DOS of the limit structures at the experimental cells. Composition of the first peaks of the valence and conduction bands for all the studied species. Valence, conduction band and band gap energies vs. composition for the monoclinic and orthorhombic mixed structures. Main geometrical parameters for all the mixed structures. "This material is available free of charge via the Internet at http://pubs.acs.org."

AUTHOR INFORMATION

Corresponding Author

* Anna Amat, Simona Fantacci, CNR-ISTM, Via Elce di Sotto 8, Perugia.

ACKNOWLEDGMENT

AA and SF thank MIUR-PRIN 2010-2011 Project No. 20104XET32 *"DSSCX" and* the CINECA award under the ISCRA initiative for the availability of high performance computing resources and support. Authors thank Paolo Umari for helpful discussions.

REFERENCES

(1) Eastaugh, N.; Walsh, V.; Chaplin, T.; Siddal, R., *The Pigment Compendium. A dictionay of Historical Pigments.* Elsevier Butterworth-Heinemann: 2004.

(2) Kühn, K.; Curran, M., *Chrome Yellow and Other Chromate Pigments*. National Gallery of Art, Washington and Cambridge University Press: 1986; p 187-218.

(3) Cove, S., *Constable*. Tate Gallery: London, 1991.

(4) Townsend, J. H., The materials of J.M.W. Turner: Pigments. *Studies in Conservation* **1993,** *38*, 231-54.

(5) Hendriks E., G. M., in Vincent Van Gogh Paintings 2: Antwerp & Paris, 1885-1888. *Eds. E. Hendriks, L. van Tilborgh* **2011,** *Waanders Publishers, Amsterdam and Zwolle,* 90-143.

(6) Jansen, L. L., H.; Bakker, N. , in Vincent Van Gogh – The Letters,. *Thames & Hudson Ltd., London and Amsterdam* **2009**.

(7) Kirby, J. S., K.; Roy, A.; Burnstock, A.; Grout, R.; White, R., *Natl. Gallery Tech. Bull.* **2003,** *28*, 4.

(8) Bomford, D. K., J.; Leighton, J.; Roy, A. , *Art in the Making: Impressionism*. National Gallery Publications: London, 1990.

(9) Butler, M. H., *Bull. Am. Inst. Conserv. Historic Artistic Works*. 1973; Vol. 13

(10) Snickt, G. V. d.; Janssens, K.; Schalm, O.; Aibéo, C.; Kloust, H.; Alfeld, M., James Ensor's pigment use: artistic and material evolution studied by means of portable X-ray fluorescence spectrometry. *X-Ray Spectrometry* **2010,** *39*, 103-111.

(11) Monico, L.; Van der Snickt, G.; Janssens, K.; De Nolf, W.; Miliani, C.; Verbeeck, J.; Tian, H.; Tan, H.; Dik, J.; Radepont, M.; Cotte, M., Degradation Process of Lead Chromate in Paintings by Vincent van Gogh Studied by Means of Synchrotron X-ray Spectromicroscopy and Related Methods. 1. Artificially Aged Model Samples. *Analytical Chemistry* **2011,** *83*, 1214-1223.

(12) Monico, L.; Van der Snickt, G.; Janssens, K.; De Nolf, W.; Miliani, C.; Dik, J.; Radepont, M.; Hendriks, E.; Geldof, M.; Cotte, M., Degradation Process of Lead Chromate in Paintings by Vincent van Gogh Studied by Means of Synchrotron X-ray Spectromicroscopy and Related Methods. 2. Original Paint Layer Samples. *Analytical Chemistry* **2011,** *83*, 1224-1231.

(13) Monico, L.; Janssens, K.; Miliani, C.; Brunetti, B. G.; Vagnini, M.; Vanmeert, F.; Falkenberg, G.; Abakumov, A.; Lu, Y.; Tian, H.; Verbeeck, J.; Radepont, M.; Cotte, M.; Hendriks, E.; Geldof, M.; Van Der Loeff, L.; Salvant, J.; Menu, M., Degradation process of lead chromate in paintings by Vincent van gogh studied by means of spectromicroscopic methods. 3. Synthesis, characterization, and detection of different crystal forms of the chrome yellow pigment. *Analytical Chemistry* **2013,** *85*, 851-859.

(14) Monico, L.; Janssens, K.; Miliani, C.; Van der Snickt, G.; Brunetti, B. G.; Guidi, M. C.; Radepont, M.; Cotte, M., Degradation Process of Lead Chromate in Paintings by Vincent van Gogh Studied by Means of Spectromicroscopic Methods. 4. Artificial Aging of Model Samples of Co-Precipitates of Lead Chromate and Lead Sulfate. *Analytical Chemistry* **2015,** *85*, 860-867.

(15) Monico, L.; Janssens, K.; Vanmeert, F.; Cotte, M.; Brunetti, B. G.; Van der Snickt, G.; Leeuwestein, M.; Plisson, J. S.; Menu, M.; Miliani, C., Degradation Process of Lead Chromate in Paintings by Vincent van Gogh Studied by Means of Spectromicroscopic Methods. Part 5. Effects of Non original Surface Coatings into the Nature and Distribution of Chromium and Sulfur Species in Chrome Yellow Paints. *Analytical Chemistry* **2014,** *86*, 10804-10811.

(16) Tan, H.; Tian, H.; Verbeeck, J.; Monico, L.; Janssens, K.; Van Tendeloo, G., Nanoscale Investigation of the Degradation Mechanism of a Historical Chrome Yellow Paint by Quantitative Electron Energy Loss spectroscopy Mapping of Chromium Species. *Angewandte Chemie International Edition* **2013**, 52, 11360 – 11363;

(17) Monico, L.; Janssens, K.; Hendriks, E.; Vanmeert, F.; Van der Snickt, G.; Cotte, M.; Falkenberg, G.; Brunetti, B. G.; Miliani, C., Evidence for Degradation of the Chrome Yellows in Van Gogh's Sunflowers: A Study Using Noninvasive In-Situ Methods and Synchrotron-Radiation-Based X-ray Techniques. *Angewandte Chemie International Edition* **2015,** *54*, 13923-13927.

(18) Monico, L.; Janssens, K.; Hendriks, E.; Brunetti, B. G.; Miliani, C., Raman study of different crystalline forms of PbCrO4 and PbCr1–xSxO4 solid solutions for the noninvasive identification of chrome yellows in paintings: a focus on works by Vincent van Gogh. *Journal of Raman Spectroscopy* **2014,** *45*, 1034-1045.

(19) Monico, L.; Janssens, K.; Cotte, M.; Romani, A.; Sorace, L.; Grazia, C.; Brunetti, B. G.; Miliani, C., Synchrotron-based X-ray spectromicroscopy and electron paramagnetic resonance spectroscopy to investigate the redox properties of lead chromate pigments under the effect of visible light. *J. Anal. At. Spectrom.* **2015,** *30*, 1500-1510.

(20) Monico, L.; Janssens, K.; Alfeld, M.; Cotte, M.; Vanmeert, F.; Ryan, C. G.; Falkenberg, G.; Howard, D. L.; Brunetti, B. G.; Miliani, C., Full spectral XANES imaging using the Maia detector array as a new tool for the study of the alteration process of chrome yellow pigments in paintings by Vincent van Gogh. *J. Anal. At. Spectrom.* **2015,** *30*, 613-626.

(21) Monico, L.; Janssens, K.; Cotte, M.; Sorace, L.; Vanmeert, F.; Brunetti, B. G.; Miliani, C., Chromium speciation methods and infrared spectroscopy for studying the chemical reactivity of lead chromate-based pigments in oil medium. *Microchem. J.* **2016**, 124, 272-282.

(22) Amat, A.; De Angelis, F.; Sgamellotti, A.; Fantacci, S., Theoretical investigation of the structural and electronic properties of luteolin, apigenin and their deprotonated species. *Journal of Molecular Structure: THEOCHEM* **2008,** *868*, 12-21.

(23) Amat, A.; Clementi, C.; Miliani, C.; Romani, A.; Sgamellotti, A.; Fantacci, S., Complexation of apigenin and luteolin in weld lake: a DFT/TDDFT investigation. *Physical chemistry chemical physics : PCCP* **2010,** *12*, 6672-6684.

(24) Amat, A.; Clementi, C.; De Angelis, F.; Sgamellotti, A.; Fantacci, S., Absorption and emission of the apigenin and luteolin flavonoids: A TDDFT investigation. *Journal of Physical Chemistry A* **2009,** *113*, 15118-15126.

(25) Amat, A.; Miliani, C.; Romani, A.; Fantacci, S., DFT/TDDFT investigation on the UV-vis absorption and fluorescence properties of alizarin dye. *Physical Chemistry Chemical Physics* **2015,** *17* (9), 6374-6382.

(26) Amat, A.; Rosi, F.; Miliani, C.; Sgamellotti, A.; Fantacci, S., Theoretical and experimental investigation on the spectroscopic properties of indigo dye. In *Journal of Molecular Structure*, 2011; Vol. 993, pp 43-51.

(27) Carta, L.; Biczysko, M.; Bloino, J.; Licari, D.; Barone, V., Environmental and complexation effects on the structures and spectroscopic signatures of organic pigments relevant to cultural heritage: the case of alizarin and alizarin–Mg(ii)/Al(iii) complexes. *Physical Chemistry Chemical Physics* **2014,** *16*, 2897.

(28) Fantacci, S.; Amat, A.; Sgamellotti, A., Computational chemistry meets cultural heritage: Challenges and perspectives. *Accounts of Chemical Research* **2010,** *43*, 802-813.

(29) Hogan, C.; Da Pieve, F., Colour degradation of artworks: an ab initio approach to X-ray, electronic and optical

spectroscopy analyses of vermilion photodarkening. *J. Anal. At. Spectrom.* **2015,** *30*, 588-598

(30) Tilocca, A.; Fois, E., The Color and Stability of Maya Blue: TDDFT Calculations. *The Journal of Physical Chemistry C* **2009,** *113*, 8683-8687.

(31) Amat, A.; De Angelis, F., Challenges in the simulation of dye-sensitized ZnO solar cells: quantum confinement, alignment of energy levels and excited state nature at the dye/semiconductor interface. *Physical Chemistry Chemical Physics* **2012,** *14*, 10662.

(32) Di Carlo, G.; Orbelli Biroli, A.; Pizzotti, M.; Tessore, F.; Trifiletti, V.; Ruffo, R.; Abbotto, A.; Amat, A.; De Angelis, F.; Mussini, P. R., Tetraaryl ZnII porphyrinates substituted at β-pyrrolic positions as sensitizers in dye-sensitized solar cells: A comparison with meso-disubstituted push-pull ZnII porphyrinates. *Chemistry - A European Journal* **2013,** *19*, 10723-10740.

(33) Salvatori, P.; Amat, A.; Pastore, M.; Vitillaro, G.; Sudhakar, K.; Giribabu, L.; Soujanya, Y.; De Angelis, F., Corrole dyes for dye-sensitized solar cells: The crucial role of the dye/semiconductor energy level alignment. *Computational and Theoretical Chemistry* **2014,** *1030*, 59-66.

(34) Singh, V. K.; Salvatori, P.; Amat, A.; Agrawal, S.; De Angelis, F.; Nazeeruddin, M. K.; Krishna, N. V.; Giribabu, L., Near-infrared absorbing unsymmetrical Zn(II) phthalocyanine for dye-sensitized solar cells. *Inorganica Chimica Acta* **2013,** *407*, 289-296.

(35) De Angelis, F.; Fantacci, S.; Selloni, A., Alignment of the dye's molecular levels with the TiO(2) band edges in dye-sensitized solar cells: a DFT-TDDFT study. *Nanotechnology* **2008,** *19*, 424002.

(36) Srimath Kandada, A. R.; Fantacci, S.; Guarnera, S.; Polli, D.; Lanzani, G.; De Angelis, F.; Petrozza, A., Role of hot singlet excited states in charge generation at the black Dye/TiO2 interface. *ACS Applied Materials and Interfaces* **2013,** *5*, 4334-4339.

(37) Nazeeruddin, M. K.; De Angelis, F.; Fantacci, S.; Selloni, A.; Viscardi, G.; Liska, P.; Ito, S.; Takeru, B.; Grätzel, M., Combined experimental and DFT-TDDFT computational study of photoelectrochemical cell ruthenium sensitizers. *Journal of the American Chemical Society* **2005,** *127*, 16835-16847.

(38) Pastore, M.; Mosconi, E.; Fantacci, S.; De Angelis, F., Computational Investigations on Organic Sensitizers for Dye-Sensitized Solar Cells. *Current Organic Synthesis* **2012,** *9*, 215-232.

(39) Giannozzi, P.; Baroni, S.; Bonini, N.; Calandra, M.; Car, R.; Cavazzoni, C.; Ceresoli, D.; Chiarotti, G. L.; Cococcioni, M.; Dabo, I.; Dal Corso, A.; de Gironcoli, S.; Fabris, S.; Fratesi, G.; Gebauer, R.; Gerstmann, U.; Gougoussis, C.; Kokalj, A.; Lazzeri, M.; Martin-Samos, L.; Marzari, N.; Mauri, F.; Mazzarello, R.; Paolini, S.; Pasquarello, A.; Paulatto, L.; Sbraccia, C.; Scandolo, S.; Sclauzero, G.; Seitsonen, A. P.; Smogunov, A.; Umari, P.; Wentzcovitch, R. M., QUANTUM ESPRESSO: a modular and open-source software project for quantum simulations of materials. *Journal of Physics-Condensed Matter* **2009,** *21* (39).

(40) Dal Corso, A., Pseudopotential periodic table: Form H to Pu. *Computational Material Science* **2014,** *95*, 337-350.

(41) Monkhorst, H. J.; Pack, J. D., Special points for Brillouin-zone integrations. *Physical Review B* **1976,** *13*, 5188-5192.

(42) Quareni, S.; De Pieri, R., A three-dimensional refinement of the structure of Coroite, PbCrO4. *Acta Crystallographica* **1965,** *19*, 287-289.

(43) Knight, K. S., A high temperature strucutal phase transition in crocoite (PbCrO4) at 1068 K: crystak structure refinement at 1073 K and thermal expansion tensor determination at 1000 K. *Mineralogical Magazine* **2000,** *64*, 291-300.

(44) Antao, S. M., Structural trends for celestite (SrSO4), anglesite (PbSO4) and barite (BaSO4): confirmation of expected variations within SO4 groups. *American Mineralogist* **2012,** *97*, 661-665.

(45) Monico, L.; Van der Snickt, G.; Janssens, K.; De Nolf, W.; Miliani, C.; Verbeeck, J.; Tian, H.; Tan, H.; Dik, J.; Radepont, M.; Cotte, M., Degradation process of lead chromate in paintings by Vincent van Gogh studied by means of synchrotron X-ray spectromicroscopy and related methods. 1. Artificially aged model samples. *Analytical chemistry* **2011,** *83*, 1214-23.

(46) Tan, H.; Tian, H.; Verbeeck, J.; Monico, L.; Janssens, K.; Van Tendeloo, G., Nanoscale investigation of the degradation mechanism of a historical chrome yellow paint by quantitative electron energy loss spectroscopy mapping of chromium species. *Angewandte Chemie - International Edition* **2013,** *52*, 11360-11363.

(47) Erkens, L.; Hamers, H.; Hermans, R.; Claeys, E.; Bijnens, M., Lead chromates: A review of the state of the art in 2000. *Surface Coatings International Part B: Coatings Transactions* **2001,** *84*, 169-176.

(48) Xiang, J.-H.; Yu, S.-H.; Xu, Z., Polymorph and Phase Discrimination of Lead Chromate Pigments by a Facile Room Temperature Precipitation Reaction. *Crystal Growth & Design* **2004,** *4*, 1311-1315.

(49) Errandonea, D.; Bandiello, E.; Segura, A.; Hamlin, J. J.; Maple, M. B.; Rodriguez-Hernandez, P.; Munoz, A., Tuning the band gap of PbCrO4 through high-pressure: Evidence of wide-to-narrow semiconductor transitions. *Journal of Alloys and Compounds* **2014,** *587*, 14-20.

(50) Bell, I.; Hill, M., Density-Functional Theory of the Energy Gap. *Physical Review Letters* **1983,** *51*, 1888-1891.

(51) Chan, M. K. Y.; Ceder, G., Efficient band gap prediction for solids. *Physical Review Letters* **2010,** *105*.

(52) Hai, X.; Tahir-Kheli, J.; Goddard, W. a., Accurate band gaps for semiconductors from density functional theory. *Journal of Physical Chemistry Letters* **2011,** *2*, 212-217.

(53) Errandonea, D.; Munoz, A.; Rodriguez-Hernandez, P.; Proctor, J. E.; Sapiña, F.; Bettinelli, M., Theoretical and Experimental Study of the Crystal Structures, Lattice Vibrations, and Band Structures of Monazite-Type PbCrO4, PbSeO4, SrCrO4, and SrSeO4. *Inorganic Chemistry* **2015,** *54*, 7524-7535.

(54) Safardoust-Hojaghan, H.; Shakouri-Arani, M.; Salavati-Niasari, M., A facile and reliable route to prepare of lead sulfate nanostructures in the presence of a new sulfur source. *Journal of Materials Science: Materials in Electronics* **2015,** *26*, 1518-1524.

(55) Clavier, N.; Podor, R.; Dacheux, N., Crystal chemistry of the monazite structure. *Journal of the European Ceramic Society* **2011,** *31*, 941-976.

(56) Suquet, H.; Launay, S., A Crystallochemical Study OF Chrome Yellow Pigments. *European Journal of Solid State and Inorganic Chemistry* **1988,** *25*, 589-598.

Structural and Electronic Properties of the $PbCrO_4$ Chrome Yellow Pigment and of Its Light Sensitive Sulfate-Substituted Compounds

Anna Amat,[a,b] Costanza Miliani,[b] Simona Fantacci [a,b,*]

[a] Computational Laboratory for Hybrid/Organic Photovoltaics (CLHYO), CNR-ISTM, via Elce di Sotto 8, 06123 Perugia, Italy.

[b] CNR-ISTM, via Elce di Sotto 8, 06123 Perugia, Italy.

Graphics for Table of Contents